WATER RESOURCES RESEARCH, VOL. 36, NO. 8, PAGES 2197–2207, AUGUST 2000

Global-scale flow routing using a source-to-sink algorithm

Francisco Olivera
Center for Research in Water Resources, University of Texas at Austin

James Famiglietti[1]
Department of Geological Sciences, University of Texas at Austin

Kwabena Asante
Center for Research in Water Resources, University of Texas at Austin

Abstract. In this paper, the development and global application of a new approach to large-scale river routing is described. It differs from previous methods by the extent to which the information content of high-resolution global digital elevation models is exploited in a computationally efficient framework. The model transports runoff directly from its source of generation in a land model cell to its sink on a continental margin or in an internally draining basin (and hence is referred to as source-to-sink routing) rather than from land cell to land cell (which we call cell-to-cell routing). It advances the development of earlier source-to-sink models by allowing for spatially distributed flow velocities, attenuation coefficients, and loss parameters. The method presented here has been developed for use in climate system models, with a specific goal of generating hydrographs at continental margins for input into an ocean model. However, the source-to-sink approach is flexible and can be applied at any space-time scale and in a number of other types of large-scale hydrological and Earth system models. Hydrographs for some of the world's major river basins resulting from a global application, as well as hydrographs for the Nile River from a more detailed application, are discussed.

1. Introduction

Large-scale river-routing algorithms are required for a range of modeling applications in global hydrology and Earth system science, including macroscale hydrological modeling, fully coupled land-ocean-atmosphere climate system modeling, terrestrial biogeochemical and ecosystem modeling, and dynamic global vegetation modeling. Their purpose is to simulate the transport of runoff generated within modeling units on land (e.g., grid cells, watersheds, or other spatially defined units), through river networks, across the landscape, to its associated delivery point on the continental margin in order to produce realistic streamflow hydrographs at any location along the length of the channel. While the representation of the vertical movement of moisture through the soil-vegetation-atmosphere system has received considerable attention in large-scale modeling efforts [*Henderson-Sellers et al.*, 1993], lateral transport has received comparatively less.

Because streamflow is an integral component of the climate system, the absence of river-routing algorithms in Earth system models represents a significant shortcoming. For example, water cycle closure is required in fully coupled climate system models (CSMs) (e.g., to maintain global freshwater and oceanic salinity balances), yet the representation of river transport that effectively closes the cycle is often primitive or nonexistent [*Boville and Gent*, 1998]. River routing provides a means for transport of not only water but sediment, nutrients, and biogeochemical materials as well, all of which are important elements of Earth system cycles on land: Hence their river-borne transport requires an appropriate model representation of streamflow routing. From a model verification perspective, streamflow is the most observable and well documented of the land surface fluxes. Because streamflow from continental watersheds represents the outflow of water from vast regions of land surface, it is an expression of the integrated response of the land to all the Earth system processes occurring within basin boundaries. Consequently, large-scale river routing provides an opportunity to better validate model simulations of terrestrial hydrology, ecology, biogeochemistry, and climate.

The availability of high-resolution global digital elevation models (DEMs) like the 5-arc-min TerrainBase [*Row et al.*, 1995] or the 30-arc-sec GTOPO30 [*Gesch et al.*, 1999] offers an important opportunity to advance the development of large-scale routing models by enabling progressively more realistic representations of topography and river channel networks. In this regard, *Oki and Sud* [1998] have developed a global raster river network with a resolution of 1° × 1° using vector maps and DEM high-resolution data. However, a significant challenge is to determine how the relatively high resolution topographic data can be utilized to enhance river routing algorithms that can be interactively coupled to regional and global climate models, which typically operate at coarser scales (e.g., 0.5° at high resolution to 4° × 5° at low resolution), without significantly increasing the often large computational overhead of the host models.

The purpose of this paper is to describe the development

[1]Also at Center for Research in Water Resources, University of Texas at Austin.

Paper number 2000WR900113.
0043-1397/00/2000WR900113$09.00

and global application of a new approach to large-scale river routing. The model transports runoff directly from its source of generation in a land model unit to its sink on a continental margin or in an internally draining basin (and hence is referred to as source-to-sink routing) rather than from land cell to land cell (which we call cell-to-cell routing). It differs from most previous methods by the extent to which the information content of high-resolution global DEMs is exploited; it advances the development of earlier source-to-sink models by allowing for spatially distributed flow velocities, flow attenuation coefficients, and loss parameters; and it is computationally more efficient than cell-to-cell models. The method presented here has been developed for use in CSMs, with a specific goal of generating hydrographs at continental margins for input into an ocean model, so that the importance of water cycle closure in coupled land-ocean-atmosphere models can be properly assessed. However, the source-to-sink approach is flexible and can be applied at any space-time scale and in a number of other types of large-scale hydrological and Earth system models.

2. Previous Work

Large-scale flow-routing models can be classified into two main groups: cell-to-cell models in which flow accounting occurs within each modeling unit and source-to-sink models in which flow accounting occurs only between the land source and its outlet point on the continental margin. In this section, previous models, their advantages and disadvantages, and applicability are briefly discussed.

2.1. Cell-to-Cell Routing

Most previous efforts at large-scale river routing have employed the cell-to-cell technique, which consists of determining the amount of water that flows from each land model cell to its neighbor downstream cell and tracking it over the river network [*Vörösmarty et al.*, 1989; *Liston et al.*, 1994; *Miller et al.*, 1994; *Sausen et al.*, 1994; *Coe*, 1997; *Hagemann and Dümenil*, 1998; *Branstetter and Famiglietti*, 1999]. This method invokes the principle of continuity to derive a mass balance of water stored within a land model cell, given, for example, by

$$\frac{dS_i(t)}{dt} = \sum_j I_{j-i}(t) - O_i(t) + R_i(t) - E_i(t), \qquad (1)$$

where S_i $[L^3]$ is the volume stored in cell i, t $[T]$ is time, $I_{j-i}[L^3/T]$ is the inflow to cell i from each of the immediately upstream neighbor cells j, $O_i[L^3/T]$ is the outflow from cell i, R_i $[L^3/T]$ is the runoff generated within cell i, and E_i $[L^3/T]$ are the losses due to evaporation and infiltration from the river network within cell i. Note that the term E_i accounts for losses during the routing process after the runoff has been generated. Outflow from the cell is typically modeled using a linear reservoir, where $S_i = K_i O_i$ and K_i $[T]$ is a parameter which represents the residence time in cell i. Determination of K_i has been further studied by *Vörösmarty et al.* [1989] to account for floodplain storage, by *Liston et al.* [1994] to account for groundwater flow, by *Coe* [1997] to include lakes and wetlands, and by *Hagemann and Dümenil* [1998] to incorporate a cascade of linear reservoirs rather than a single storage component.

Advantages of cell-to-cell schemes include the ease with which they can be implemented globally (e.g., *Miller et al.* [1994], *Sausen et al.* [1994], *Coe* [1997], *Hagemann and Dümenil* [1998], *Branstetter and Famiglietti* [1999], and *Fekete et al.* [1999] have all reported reasonable results in global applications) and explicitly account for the volume of river water in each cell. This second advantage enables hydrograph computation for any land cell of interest. Additionally, if the volume of river water stored in the cell can be transformed into a fraction of land area covered by surface water (i.e., wetlands, floodplain storage, rivers, lakes, or reservoirs [*Coe*, 1997]), then the effect of that surface water on land-atmosphere interaction can be simulated by the climate model [*Bates et al.*, 1993; *Hostetler et al.*, 1993, 1994; *Bonan*, 1995].

However, cell-to-cell routing schemes possess some significant disadvantages that, in part, have motivated the present research. Primary among these is that the cell-to-cell method does not account for within-cell routing, which clearly impacts the outflow hydrograph for the coarser grid associated with climate models [see, e.g., *Naden*, 1993]. In other words, it does not consider the routing of water from the different areas of the cell to the cell outlet, from which it is routed to its downstream cell. In order to capture these important within-cell effects, due to higher-resolution variations in topography that define river networks, cell-to-cell algorithms could simply be run at the higher resolution of currently available global DEMs (e.g., roughly 1 km for GTOPO30). However, because there are more than 90,000 DEM cells in a typical climate model cell (i.e., approximately 2.8° resolution), this is computationally infeasible for routing schemes that will be interactively coupled within climate models, given the significant computational overhead. Additionally, running cell-to-cell algorithms at the climate model grid resolution also limits the accuracy with which river networks and watershed boundaries can be delineated, since grid cells have to be assigned entirely to one, and only one, watershed. In short, cell-to-cell methods, in their current form, cannot readily capitalize on the best available global DEMs in order to more accurately route streamflow across the continents into the oceans.

2.2. Source-to-Sink Routing

In their effort to develop more efficient routing models that do not spend resources in flow and storage calculations at locations in which the modeler is not interested, researchers developed (what is herein referred to as) source-to-sink models. In the literature, researchers refer to routing from "cells in which runoff is produced" to "watershed outlet cells." In this paper, cells in which runoff is produced are called source cells or just sources, and watershed outlet cells are called sink cells or sinks.

Naden [1993] describes a routing method that implicitly includes within-source routing (i.e., routing from the different areas of the source to the source outlet) followed by source-to-sink routing (i.e., routing from the source outlet to the watershed outlet). Runoff from each source is convolved with a source-specific response function to determine the contribution of each source to streamflow at the sink. Total streamflow at the sink at any time is the sum of the contributions from all sources in the watershed. Although presented as a large-scale hydrologic model, the approach was only tested in a 10,000-km^2 watershed. Still, according to the author, the fact that network width functions can be determined from high-resolution global DEMs using Geographic Information Systems (GIS) suggests that the method is likely to be applicable globally.

Lohman et al. [1996] employ a response function for within-source routing and the linearized St. Venant equation to trans-

port streamflow from the source outflow point to the sink. The response function for within-source routing is not specific to each source and is equivalent to *Mesa and Mifflin*'s [1986] hillslope response. It is obtained by deconvolution of the catchment response function with the river network response function, which is conceptually similar to the network width function of *Mesa and Mifflin* [1986]. The scheme relies heavily on the availability of runoff data globally for the deconvolution of functions and, as such, may only be applicable on a regional basis at present (e.g., *Lohman et al.* [1996] test the method in the 38,000-km^2 Weser River catchment in Germany, and *Lohman et al.* [1998] apply the scheme in the 566,000-km^2 Arkansas Red River basin). However, the authors intend to simplify and regionalize grid cell response calculations to increase the domain over which their approach can be applied.

Kite et al. [1994] described the development of a method that consists of source-to-sink routing within each source, followed by cell-to-cell routing in the watershed, and its application in the 1,600,000-km^2 Mackenzie River basin. The watershed was partitioned into a number of sources, or grouped response units (GRUs), and further subdivided into five different land cover types. The distribution of travel times to the GRU outlet was computed for each land cover type by computing the travel time from each pixel to the GRU outlet (calculated as the sum of a to-stream and in-stream travel time). Nonlinear reservoir inflow-storage and outflow-storage relationships were used to transport streamflow from GRU outlets to the next GRU downstream. The approach described in our paper most closely resembles the within-GRU component of *Kite et al.* [1994] with important modifications and simplifications appropriate for application at the global scale.

Advantages and disadvantages of our source-to-sink model with respect to the previously described routing schemes are as follows. The first advantage is that it uses the river network topology generated within GIS from raster high-resolution spatial data (i.e., GTOPO30 and future higher-resolution DEMs) and analyses it with built-in GIS tools for estimating the response function parameters of the lower-resolution modeling units used in global climate models. A second advantage is that our source-to-sink model accommodates spatially variable streamflow parameters. The source-to-sink models described above require uniform parameters, which is an important shortcoming for large-watershed flow routing. A third advantage of the source-to-sink model presented here is that the streamflow parameters (i.e., flow velocity, attenuation coefficient, and loss parameter) and the resulting hydrographs are scale-independent. This implies that the input parameters do not have to be recalibrated when the resolution of the modeling units changes. It also implies that the accuracy of the model results improve as the resolution of the modeling units increases. This is not necessarily true for cell-to-cell models, as it has been recently demonstrated that cell resolution affects flow attenuation [*Olivera et al.*, 1999]. A final advantage is computational efficiency relative to the cell-to-cell approach. Because streamflow is transported directly from the point of runoff generation to the watershed outlet, routing calculations are not required within all the land cells between these two endpoints. The importance of this computational efficiency increases for larger watersheds and higher-resolution applications. An important disadvantage of the source-to-sink method is that river water stored within each cell is not explicitly tracked in time; consequently, hydrographs are only generated at watershed outlets rather than for every cell on the land surface as in the cell-to-cell method. Finally, because of the linearity of the system, the source-to-sink model requires constant in time, but not necessarily uniform in space, flow parameters (i.e., flow velocity, flow attenuation coefficient, and loss coefficient), so that response functions can be defined for each source.

In our opinions the advantages of the source-to-sink approach outweigh the disadvantages and hence justify an exploration of the feasibility of the approach at the global scale in the context of an eventual coupling with a CSM. The remainder of this paper describes the global implementation of a simple and robust source-to-sink routing scheme. A detailed intercomparison of cell-to-cell and source-to-sink methods is an active area of research by the authors, as are methods for combining the two approaches. Results of these investigations will be presented in future publications.

3. Methodology

The methodology presented here models the process by which the water moves across the landscape from the location where runoff is generated, the source, to the location along the continental margin where no further flow routing is necessary, the sink. The model assumes that the terrain topography is described by a DEM, and the runoff distribution, in space and time, is known from a separate land surface model. It generates hydrographs at the different sinks.

The model is supported by a Global Spatial Database, in the form of raster and vector GIS maps, specifically developed to work in conjunction with it. Streamflow parameters, such as velocity, attenuation coefficients, and loss parameters, which depend more on local than on overall topographic conditions, are not included in the database and are left for the user to define.

3.1. Global Spatial Database

In this section, the general principles followed to develop the Global Spatial Database that supports the model are explained. This Global Spatial Database is available from the authors by request.

A DEM is a sampled array of elevations for ground positions that usually are at regularly spaced intervals. DEM-based terrain analysis consists of extracting from the DEM the relevant information about the flow network for hydrologic modeling. GTOPO30, a set of 30-arc-sec (approximately 1 km) DEMs, was used for the hydrologic analysis because it is the highest-resolution raster topographic data available for the entire world. The terrain analysis was carried out by applying standard GIS functions included in commercially available software that supports operations on raster data.

By identifying the downstream pixel adjacent to each terrain pixel, a network that represents the flow paths is produced, and a unique path can be traced from each pixel to the ocean (see Figure 1). In order for water to flow along the landscape without being trapped in terrain depressions, each pixel must have at least one of its eight neighbor pixels at a lower elevation. However, in some cases, terrain models (DEMs) depict fictitious depressions, produced by the interpolation schemes used to describe variation in elevation between raster points [*DeVantier and Feldman*, 1993]. In general, the existence of depressions in the DEM is explained by (1) fictitious terrain depressions, also called pits, which might be small for most practical purposes but which are critical for hydrologic mod-

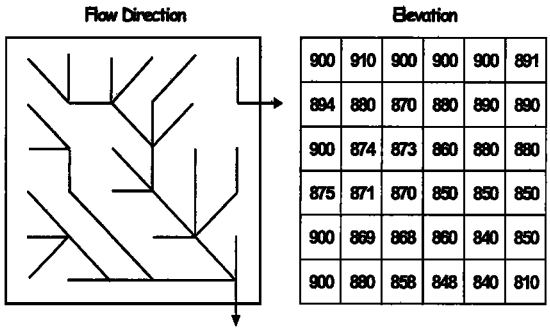

Figure 1. Flow directions and flow paths for the elevation model shown.

eling, and (2) inland catchments in which the lowest pixel constitutes a pour point (i.e., a point toward which water in the surrounding area flows and forms lakes or ponds). Therefore, before determining the flow network, it is necessary to correct the DEM by filling the pits up to an elevation that allows water to flow through and by flagging the lowest pixels of the inland catchments (pour points) as water sinks. The methodology used to identify inland catchments consists of filling all the DEM depressions as if they were pits and comparing the filled areas with maps of basins of the world available in the literature [*UNESCO*, 1978; *Revenga et al.*, 1998]. The lowest pixel of each of the filled areas that coincide with an inland catchment is flagged as a water sink, and these pixels constitute the catchment pour points. With all the pour points identified, the DEM pits are filled, and the flow network is determined. Once the flow network has been determined, sinks and sources can be defined.

Sinks are runoff-receiving units and are defined as the areas where the water needs no further routing, because it has either discharged into the ocean or into lakes located in terrain depressions. These areas are located along the continental margin (coastline pixels) and at the lowest elevation of the inland catchments (pour point pixels). After subdividing the entire globe into square boxes by a 3° × 3° (longitude by latitude) mesh, a resolution typical of ocean circulation models, sinks are defined as those boxes containing coastline segments or inland catchment pour points. Most sinks are located along the coastline, whereas inland catchment pour points are less common. All other boxes are not considered sinks because water flows through them (see Figure 2 for an example of the African continent).

Sources are runoff-producing units and are the areas where the water enters the surface water system as runoff. To define the source polygons, three sets of polygons are intersected: (1) the drainage area of each sink delineated according to the flow network determined previously (see Figure 2 for an example of the African continent), (2) land boxes defined by subdividing the terrain into square boxes by a 0.5° × 0.5° (longitude by latitude) mesh, and (3) runoff boxes defined by a T42 mesh [*Bonan*, 1998], with resolution of approximately 2.8° × 2.8° (longitude by latitude), for which runoff time series are provided from a CSM. A fine 0.5° × 0.5° mesh is used for land boxes, rather than a coarse T42 mesh, to allow for better definition of the spatial distribution of flow times to the sink, which would otherwise be averaged over the large T42 cells. By doing this, each T42 cell is subdivided into more than 30 land boxes, allowing the routing model to better capture the geomorphological characteristics of the area. Note that the smaller land boxes are not intended to improve the resolution of the runoff distribution, which is given by a CSM with a T42 resolution. Eventually, as the resolution of climate models increases, the runoff boxes and land boxes will coincide. After intersecting the drainage area of the sinks with the mesh of land boxes and the mesh of runoff boxes, the source polygons are obtained in such a way that for each source its exact location, its runoff time series, and its corresponding sink are known (see Figure 3 for an example in the Nile River basin). In Figure 3, runoff boxes are displayed as background open and shaded, while source polygons are displayed with a thin solid outline and, because they are the product of the intersection of different polygon sets, with no regular shape.

For the African continent, for example, 120 sinks, 10,389 land boxes, and 379 runoff boxes were defined for a total of 18,372 sources. The area of the sources ranged from 0.06 to 3105 km^2 with an average value of 1600 km^2. The number of sources that drain to a specific sink ranged from 1 (for many coastal regions) to 1844 (Congo River basin) with an average value of 153. After sources and sinks have been defined, a flow-routing algorithm is used to model the motion of water from the former to the latter.

3.2. Flow-Routing Algorithm

Routing of runoff along a flow path, from the point it enters the system (source) to the point where it needs no further routing (sink), is accomplished by applying the advection-dispersion equation to flow path segments and then convolving the responses of the different segments to produce the source response at the sink [*Olivera and Maidment*, 1999]. The hydrograph for a specific sink is calculated as the sum of the contributions of all the sources that drain to it. Mathematically, this is written as

$$Q_i(t) = \sum_j Q_j(t), \tag{2}$$

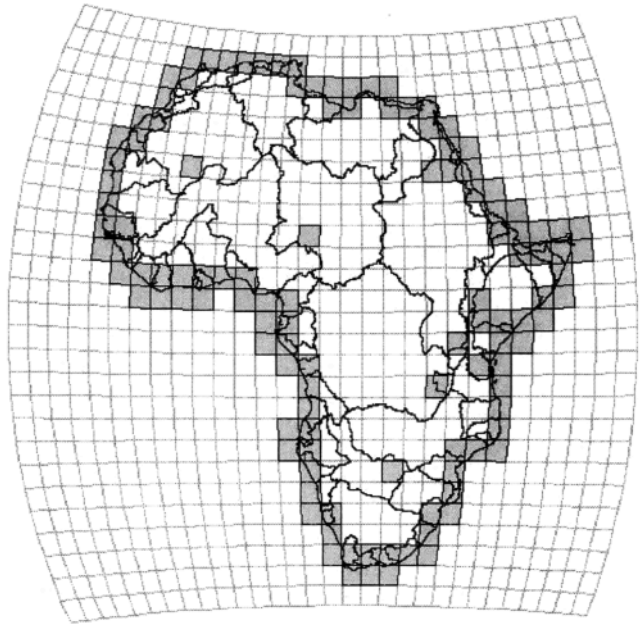

Figure 2. Sinks (shaded) and their corresponding drainage areas. For the African continent, 120 sinks were identified.

where $Q_i(t)$ $[L^3/T]$ is the hydrograph of sink i, $Q_j(t)$ $[L^3/T]$ is the contribution of source j, and the sum applies to all sources that drain to sink i. In turn, $Q_j(t)$ is calculated as

$$Q_j(t) = A_j R_j(t) * u_j(t) \tag{3}$$

where A_j $[L^2]$ is the area of source j, $Rj(t)$ $[L/T]$ is the time series of runoff generated at source j, $u_j(t)$ $[1/T]$ is the response function of source j at sink i, and the asterisk stands for the convolution integral. Assuming the response function is a first-passage-time distribution, which is in accordance with the work of other researchers who have modeled the time spent by water in surface water systems [*Mesa and Mifflin*, 1986; *Naden*, 1992; *Troch et al.*, 1994; *Olivera and Maidment*, 1999], then

$$u_j(t) = \frac{1}{2t\sqrt{\pi(t/t_j)/\prod_j}} \exp\left\{-\frac{[1-(t/t_j)]^2}{4(t/t_j)/\prod_j}\right\}, \tag{4}$$

where t_j $[T]$ is the average flow time and Π_j is a representative Peclet number for the flow path from source j to its corresponding sink i. Figure 4 shows first-passage-time distributions for different values of Π_j and $t_j = 100$ s. If, because of the spatial variability of the system, the flow path is subdivided into a sequence of segments with different flow parameters, then the values of t_j and Π_j can be calculated as [*Olivera and Maidment*, 1999]

$$t_j = \sum_k \left(\frac{1}{v_k}\right) L_k, \tag{5}$$

$$\prod_j = \left[\sum_k \left(\frac{1}{v_k}\right) L_k\right]^2 \Big/ \left[\sum_k \left(\frac{D_k}{v_k^3}\right) L_k\right], \tag{6}$$

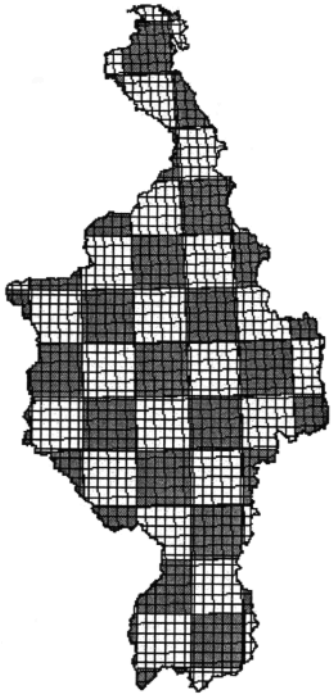

Figure 3. Source polygons defined after intersecting the drainage area of the sinks with the mesh of land boxes and the mesh of runoff boxes. For the Nile River basin, 1120 land boxes (0.5° × 0.5° longitude by latitude) and 62 runoff boxes (T42) were identified. Large open and shaded boxes correspond to the runoff boxes. It can be seen that about 30 land boxes are contained in a runoff box.

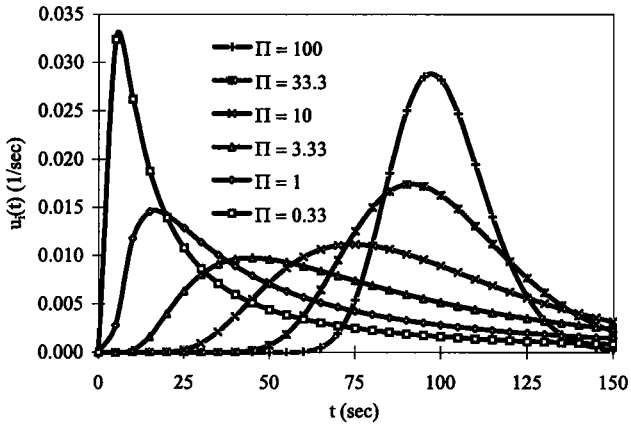

Figure 4. First-passage-time distributions for a mean value of 100 s and Peclet numbers ranging from 0.33 to 100. Note that as the Peclet numbers increases, the responses decrease their standard deviation (i.e., tend to pure translation).

where L_k $[L]$ is the flow distance, v_k $[L/T]$ is the flow velocity, and D_k $[L^2/T]$ is the attenuation coefficient in segment k of the flow path, and the sum applies to all segments of the flow path. Note that in the context of raster terrain data, flow path segments are the links that connect pixels with their immediate downstream neighbors. Thus spatially distributed flow parameters such as flow velocity and attenuation coefficient can be stored in the same raster format as the DEM.

Since the representative Peclet number Π_j is a measure of the relative importance of advection with respect to hydrodynamic dispersion (the cause of flow attenuation), some important conclusions can be drawn from (6): the relative importance of advection with respect to flow attenuation increases with flow path length and flow velocity and decreases with the attenuation coefficient. Therefore it is expected that flow attenuation plays a lesser role as the watershed size increases.

First-order losses (i.e., flow lost proportional to actual flow) can also be included in this approach by multiplying the response function of (4) by a dimensionless loss factor Φ_j [*Olivera*, 1996] (available at www.ce.utexas.edu/prof/olivera/disstn/abstract.htm) equal to

$$\Phi_j = \exp\left\{-\sum_k \left(\frac{\lambda_k}{v_k}\right) L_k\right\}, \tag{7}$$

where the loss parameter λ_k $[1/T]$ is related to the loss mechanisms such as evaporation to the atmosphere or infiltration to the deep subsurface system. The loss parameter can be understood as the fraction of water lost per unit time and reflects the fact that losses increase with flow time and that distant sources experience more losses than those located close to the sink. Note that although the loss parameter is constant, water losses are not constant and change in time as the flow changes. After accounting for losses, the source response function at the sink is equal to

$$u_j(t) = \frac{\Phi_j}{2t\sqrt{\pi(t/t_j)/\prod_j}} \exp\left\{-\frac{[1-(t/t_j)]^2}{4(t/t_j)/\prod_j}\right\}. \tag{8}$$

The summation terms in (5), (6), and (7) can be calculated using GIS functions. The flow distance from a DEM pixel to the continental margin or inland catchment pour point, for example, is calculated along the flow path according to the flow

path network determined previously and is equal to $\Sigma_k L_k$. Similarly, the summation terms $\Sigma_k L_k/v_k$, $\Sigma_k D_k L_k/v_k^3$, and $\Sigma_k \lambda_k L_k/v_k$ are calculated using the same algorithm but after multiplying L_k by weight factors equal to $1/v_k$, D_k/v_k^3, and λ_k/v_k, respectively. Therefore, after making these calculations, sources can be attributed with the average value within the polygons of $\Sigma_j L_k$ (flow length), $\Sigma_k L_k/v_k$ (flow time), $\Sigma_k D_k L_k/v_k^3$ (attenuation), and $\Sigma_k \lambda_k L_k/v_k$ (losses). Thus the smaller the source polygons are, the less the averaging affects the parameters but at the expense of more computational time.

In summary, after calculating the summation terms and attributing the source polygons with their average values, the parameters t_j, Π_j, and Φ_j are determined using (5), (6), and (7). A response function for each source is then determined using (8). The contribution of a source at its sink is obtained by convolving the response function and the runoff time series as in (3). Finally, the flow at the sink is calculated as the sum of the contributions of the sources in its drainage area as presented in (2).

4. Application, Results, and Discussion

In this section, we first demonstrate the applicability of the model for use in global routing calculations and then highlight its power and flexibility in an application in the Nile River basin.

4.1. Application to the Globe

A 10-year daily time series of T42-resolution global runoff data, simulated using the National Center for Atmospheric Research Community Climate Model Version 3 (CCM3) [*Kiehl et al.*, 1998] with an interactive land surface component, the Land Surface Model Version 1 (LSM) [*Bonan*, 1996], was used as input to our flow-routing model. While it is well known that climate model runoff does not agree well with observations, *Bonan* [1998] and *Kiehl et al.* [1998] have shown improvement in simulated hydrology over previous CCM versions in which land surface conditions were prescribed. For our purposes, use of the CCM3 runoff output is sufficient for demonstrating the features of the routing algorithm, as this is precisely the resolution and quality of runoff data that will be input into the routing scheme when coupled to a CSM.

Routing of CSM runoff data, with specified streamflow parameters, for different basins can be seen in Figure 5. The river basins selected were the Congo in Africa, the Amazon, Orinoco, and Parana in South America, the Mackenzie and Mississippi in North America, and the Yangtze and Huang Hu in Asia. In all cases, $v = 0.3$ m/s, $D = 0$, and $\lambda = 0$, which implies pure translation at a rate of 0.3 m/s and no losses. Note that we have not attempted a global calibration of these streamflow parameters, because validating CCM3 runoff is not the focus of this paper. Rather, our intention is to show the capability of the model to transport streamflow over vast land regions and simulate hydrographs at continental margins for input into ocean circulation models, given a set of streamflow parameters and simulated runoff rates.

Figure 5 shows, for all cases, lagging and damping of the flow hydrograph with respect to the runoff, so that peak flows are lower than peak runoff values, low flows are higher than low runoff values, and, in general, the entire flow hydrograph is shifted to the right, along the time axis, with respect to the runoff. The lags are induced by overall travel times to the coast, and the damping is induced by the differential travel times and by the flow attenuation processes. It can also be observed that, depending on the size, shape, and geomorphology of the watershed, lags can be as long as 4 to 5 months and damping can be as much as 40%. Note that these results are also sensitive to the choice of streamflow parameters and the spatial-temporal variability of the runoff input.

Owing to inadequacies of the climate model runoff mentioned above, we are not able to validate the imposed translation and attenuation. However, the predicted hydrographs are certainly reasonable given the realistic nature of the velocity and topographic input parameters. The impact of these delays on ocean circulation and ocean-atmosphere interaction is the subject of ongoing research.

The power and flexibility of the routing scheme, that is, its ability to incorporate terrain spatial variability, are discussed next in an application of the model to the Nile River basin under differing streamflow parameters.

4.2. Application to the Nile River Basin

Spatially distributed streamflow parameters, such as flow velocity, attenuation coefficient, and loss coefficient, are difficult to estimate at a global scale when detailed descriptions of the terrain are not available. Assumptions of uniformly distributed parameters, though appealing for their simplicity, may overlook well-known hydrologic processes that take place in some parts of the river basins. For example, floodplain storage, which is significantly important in flat areas such as the Sudd Marshes of the Nile River basin in North Africa, the Inner Delta of the Niger River basin in West Africa, and most of the Amazon River basin in South America but which is almost negligible in mountainous areas, indicates the need for accounting for nonuniformly distributed parameters.

An application of the model to the Nile River basin is included next. The Nile River drains areas from nine African countries: Burundy, Democratic Republic of the Congo, Egypt, Eritrea, Ethiopia, Kenya, Rwanda, Sudan, and Uganda. It is a 3,250,000-km^2 drainage area located in northeast Africa [*Revenga et al.*, 1998] and extends from 22°E to 40°E longitude and 3°S to 33°N latitude (see Figure 6). The Nile River at the Mediterranean derives from the confluence of the White Nile and the Blue Nile at Khartoum, Sudan. From its uppermost headstream, the Luvironza River in Burundi, the Nile has a length of more than 6700 km. The White Nile rises in the East African Highlands and flows predominantly northward. Along its way toward the confluence with the Blue Nile the White Nile flows through a large marshy region in south Sudan known as the Sudd Marshes. The Sudd are a 300-km-long by 350-km-wide, flat, and shallow plain that drains 1,560,000 km^2 and collects more than 70% of the basin precipitation. The marshes slow down the river so that about half the inflow is lost to evaporation [*Hurst and Phillips*, 1938]. The Blue Nile flows northwestward from the Ethiopian highlands. It drains 310,000 km^2 and collects approximately 15% of the precipitation of the entire basin. The Blue Nile is characterized by steep slopes, having a vertical drop of 2400 m in a distance of 1200 km. Precipitation in the Nile basin ranges from 2100 mm/yr in the Blue Nile headwaters to as much as 1200 mm/yr in the upper White Nile area to almost zero in northern and central Egypt. Most of the precipitation occurs during July and August, whereas December and January are relatively dry.

For the sink that captures the Nile River basin, the Mediterranean outfall grid cell, 1808 sources were identified with areas ranging from 0.12 km^2 to 3105 km^2 for a total of 3,350,000 km^2

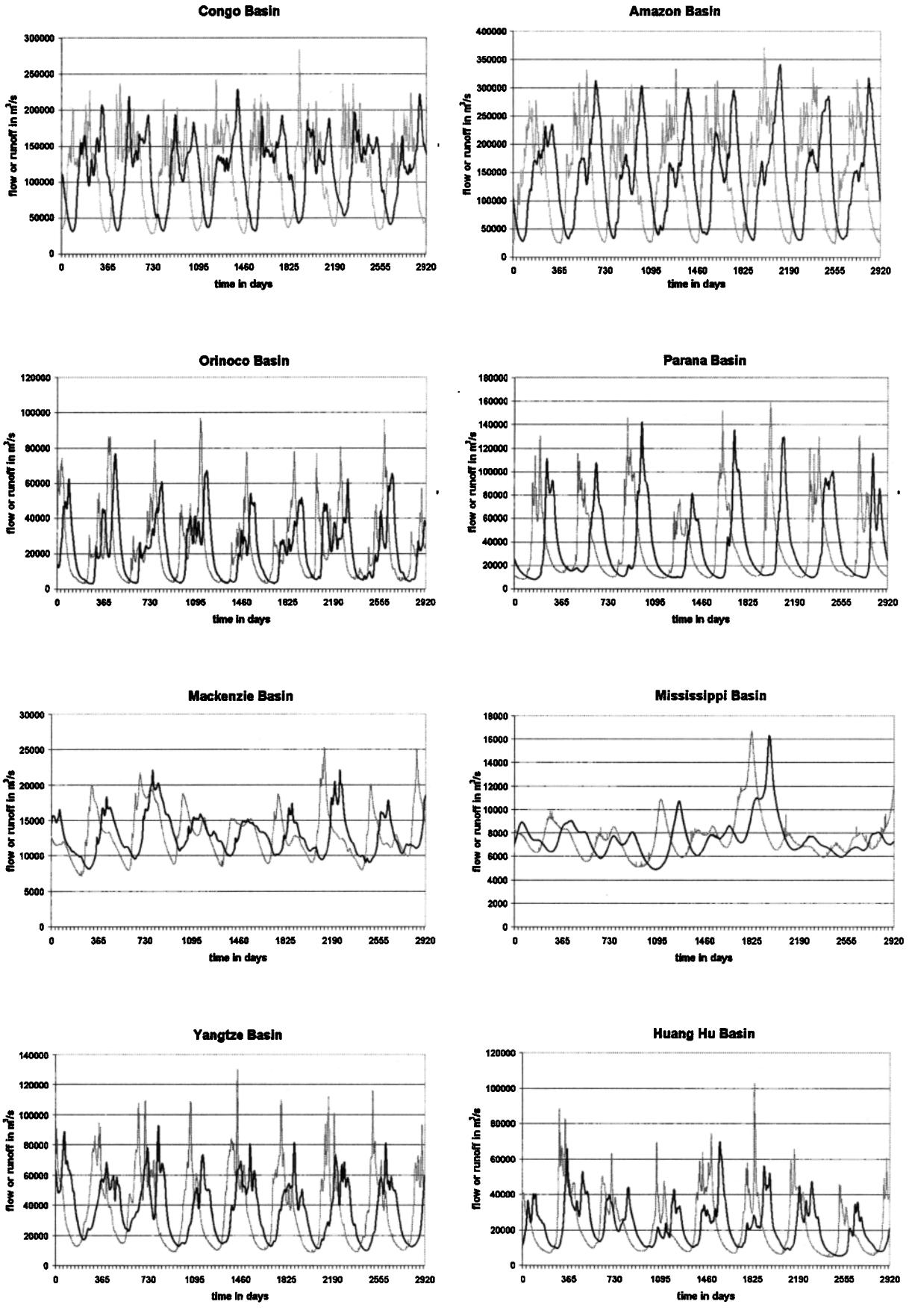

Figure 5. Simulated multiannual hydrographs for eight large watersheds of the world, assuming pure translation at a rate of 0.3 m/s and no losses.

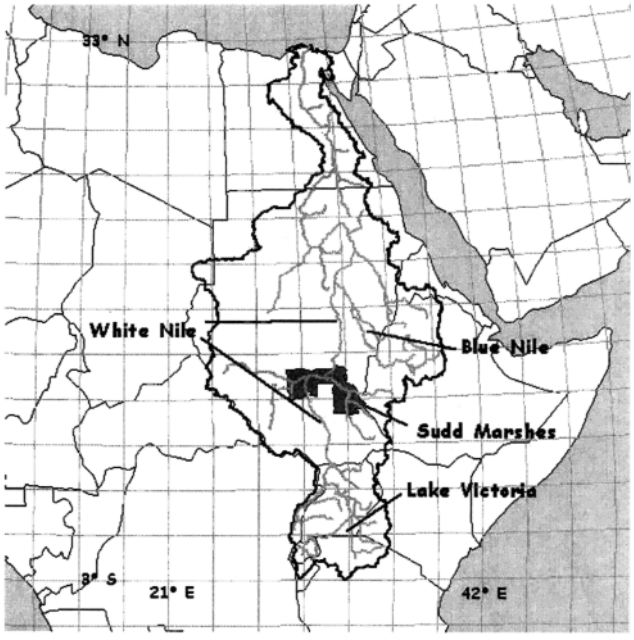

Figure 6. Nile River basin in East Africa.

(see Figure 3). This area is close to that reported by *Revenga et al.* [1998], which was estimated using a different methodology.

In this application, emphasis has been placed on the importance of accounting for the spatial variability of the streamflow parameters. For this purpose, three distinct zones were assumed to constitute the basin: the Blue Nile subbasin, the Sudd Marshes, and the rest of the basin (see Figure 7). The Blue Nile is a relatively steep area in which velocities are assumed to be higher and attenuation coefficients are assumed to be lower than in the rest of the basin. In contrast, the Sudd Marshes is a swampy area in which velocities are lower, attenuation coefficients are higher, and loss parameters are large compared to the rest of the basin. Losses were considered only in the Sudd Marshes, which has been identified as the major area of losses in the basin [*Hurst and Phillips*, 1938].

Estimation of flow velocities and loss coefficients was based on flow observations. Observed flows [*Hurst and Phillips*, 1938] indicate that peak discharges take approximately 4 days to travel 418 km, along the Blue Nile, from Wad el Aies to Khartoum, that is, a flow velocity of approximately 1.2 m/s. Likewise, the White Nile takes about 3 months to travel 711 km, predominantly through the Sudd Marshes in the Sudan from Mongalla to Malakal, that is, a velocity of about 0.1 m/s. Finally, the velocity between Malakal and Mogren, just south of Khartoum, is estimated from a distance of 794 km and a travel time of 20 days, that is, a flow velocity of approximately 0.5 m/s. The value of 0.018/day for the loss coefficient in the Sudd Marshes (i.e., a loss of 1.8% of the flow per day) was chosen to satisfy the condition of 50% losses in the area. Attenuation coefficients are order of magnitude estimates based on measured values for different river basins reported by *Fischer et al.*, [1979] and *Seo and Cheong* [1998]. After comparing hydrologic characteristics of the Nile basin zones (i.e., flow rate and slope) with those of the rivers reported in the literature, attenuation coefficients of 300 m^2/s, 4500 m^2/s, and 1500 m^2/s were chosen for the Blue Nile, the Sudd Marshes, and the rest of the Nile basin, respectively. These parameters fall within reasonable limits for flow velocities, attenuation coefficients and loss parameters and were chosen to demonstrate the importance of accounting for the spatial variability of streamflow parameters in the calculation of flows. Not all the features of the basin were considered, though, since reservoirs and lakes, which are expected to have different streamflow parameters, were not considered in the present study.

Figure 8 shows the area–flow time distribution for the Nile River basin under four different assumptions: (1) variable v and D, (2) variable v and uniform D (D = 908 m^2/s), (3) uniform v (v = 0.43 m/s) and variable D, and (4) uniform v (v = 0.43 m/s) and D (D = 908 m^2/s), where variable refers to the spatially differing values indicated above. For variable v and D the mean and standard deviation of the distribution were 100 and 49 days, respectively. The velocity, v = 0.43 m/s, used for uniform velocity analysis was chosen so that the mean of the distribution remain unaltered. The attenuation coefficient, D = 908 m^2/s, used for uniform attenuation coefficient analysis, was chosen so that the standard deviation remain unaltered when variable velocities were considered (curve 2). However, it was observed that with uniform velocities (curves 3 and 4), the standard deviation dropped to 40 days. This drop in the standard deviation value results from the fact that while the mean of the distribution depends on v only, the standard deviation depends on both v and D. From the physical point of view the basin response function or instantaneous unit hydrograph (i.e., the hydrograph at the basin outlet produced by a unit instantaneous and uniformly distributed runoff input) is a rescaled version of the area–flow time distribution. That is, the basin response function is obtained by multiplying the area (of the area–flow time distribution) by a unit instantaneous and uniformly distributed runoff input. The concept of response function,

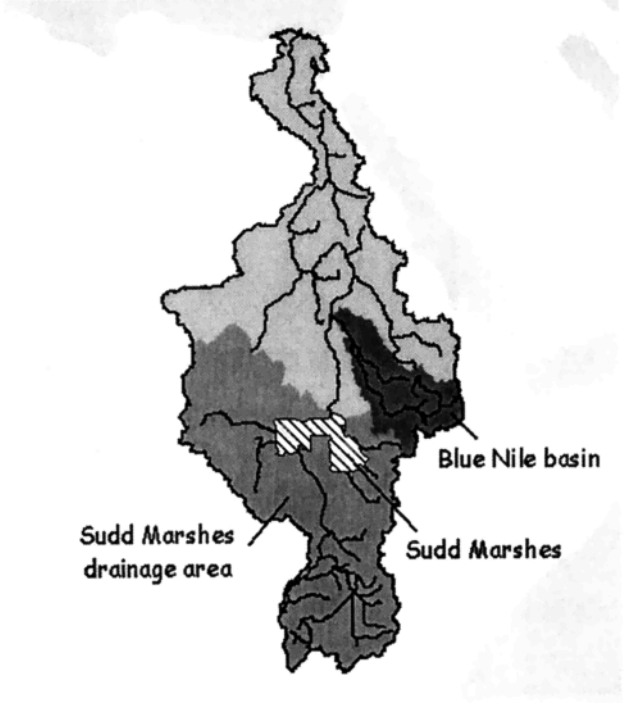

Figure 7. Hydrologic zones of the Nile River basin: the Blue Nile subbasin (dark shading), the Sudd Marshes (hatched area), and the rest of the basin (medium and light shading). The Sudd Marshes contributing drainage area (shaded) is shown here for illustration purposes, but it was not treated as a different hydrologic zone.

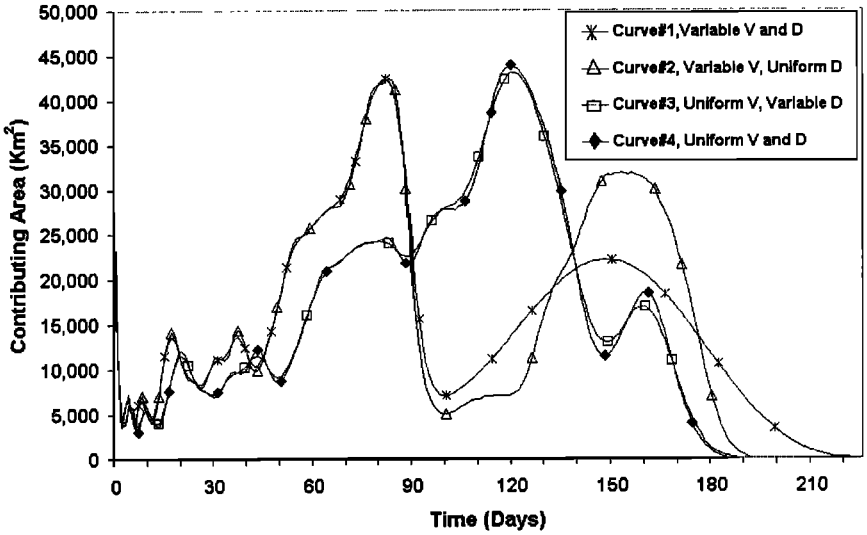

Figure 8. Contributing area-time distribution for the Nile River basin under different assumptions of flow velocity and flow attenuation coefficient.

though, is not in frequent use in large-scale hydrology since uniformly distributed runoff inputs are unlikely in large basins.

The most striking result observed in Figure 8 is that curves from the variable-velocity analysis (curves 1 and 2) and curves from the uniform-velocity analysis (curves 3 and 4) group together, while the differences between the curves within each group are minor. Curves that correspond to variable velocity are bimodal, with a first peak deriving mostly from the Blue Nile drainage area and a second deriving from the White Nile.

Spatial variability of attenuation coefficients also proved to be important, especially for the case of variable velocity, although not as important as for flow velocity. In Figure 8, curves 1 and 2 do not show much discrepancy until about day 90, when curve 1 (variable v and D) became considerably smoother than curve 2 (variable v and uniform D). Thus the effect of the difference in attenuation coefficients between curves 1 and 2 seems to be negligible for the Blue Nile drainage area (first peak) and significant for the White Nile drainage area (second peak). This additional attenuation is explained by the effect of the Sudd Marshes, characterized by very slow velocities. Similarly, the discrepancy between curves 3 (uniform v and variable D) and 4 (uniform v and D) shows up only after about day 150, when the peak and low values of curve 4 are attenuated. Because that part of the curve corresponds to the upper White Nile drainage area, the additional attenuation in curve 3 is explained by the effect of the Sudd Marshes. Still, it can be noted that for uniform velocity, the effect of flow attenuation is not significant.

It is important to note that in the area–flow time curves discussed above, the relative importance of the sources, given by the total runoff depth and overall losses, was not considered. The effect of spatial variation of runoff depth plus the temporal distribution of runoff will be considered next when generating hydrographs at the ocean. Figure 9 shows 1 year of flows at the Nile River mouth resulting from running the model, with CSM runoff data, under five sets of streamflow parameters: (1) variable v, D, and λ; (2) variable v, uniform D (D = 908 m^2/s), and variable λ; (3) uniform v (v = 0.43 m/s) and variable D and λ; (4) uniform v (v = 0.43 m/s) and D (D = 908 m^2/s) and variable λ; and (5) variable v and D with λ = 0, where variable refers to the spatially distributed values indicated above. Table 1 summarizes the results of these five model runs.

In Figure 9a, curves 1 and 2 are compared. Averaging D with a variable velocity field results in higher peak flows and lower low flows. Similarly, in Figure 9b, curves 3 and 4 are compared. Again, averaging D with a uniform velocity field results in higher peak flows and lower low flows. Finally, in Figure 9c, curves 1 and 4 are compared. As might be expected, averaging both streamflow parameters results in higher peak flows and lower low flows. In this last case, flow volume also changes because with variable velocity water stays longer in the Sudd Marshes and is subject to greater losses. The effect of accounting for losses in the Sudd Marshes is shown in Figure 9d. It can be seen that, as an average, the flow volume decreases by about 40% when λ = 0.018/day.

The discrepancies between the hydrographs, peak flows, and low flows in Figure 9 show the importance of accounting for localized areas of floodplain storage and, in general, of accounting for spatial variability of the terrain and streamflow parameters. The fact that a 108,000-km^2 localized area of floodplain storage, like the Sudd Marshes, can modify peak flows by as much as 32% in a 3,250,000-km^2 basin shows that models that do not support spatially distributed streamflow parameters are limited in their applicability.

5. Conclusions

A model for runoff routing at a global, continental, or large-watershed scale has been developed. The method presented here has been developed for use in CSMs, with a specific goal of generating hydrographs at continental margins for input into an ocean model so that the importance of large-scale river transport can be properly assessed. It models the transfer of runoff from its sources of generation (where it enters the surface water system) to its sinks at either the continental margin or an inland catchment pour point (where no further routing is necessary) and therefore is referred to as a source-to-sink model. The model is supported by a Global Spatial Database in which all sources and sinks for land areas of the entire world have been identified and properly attributed.

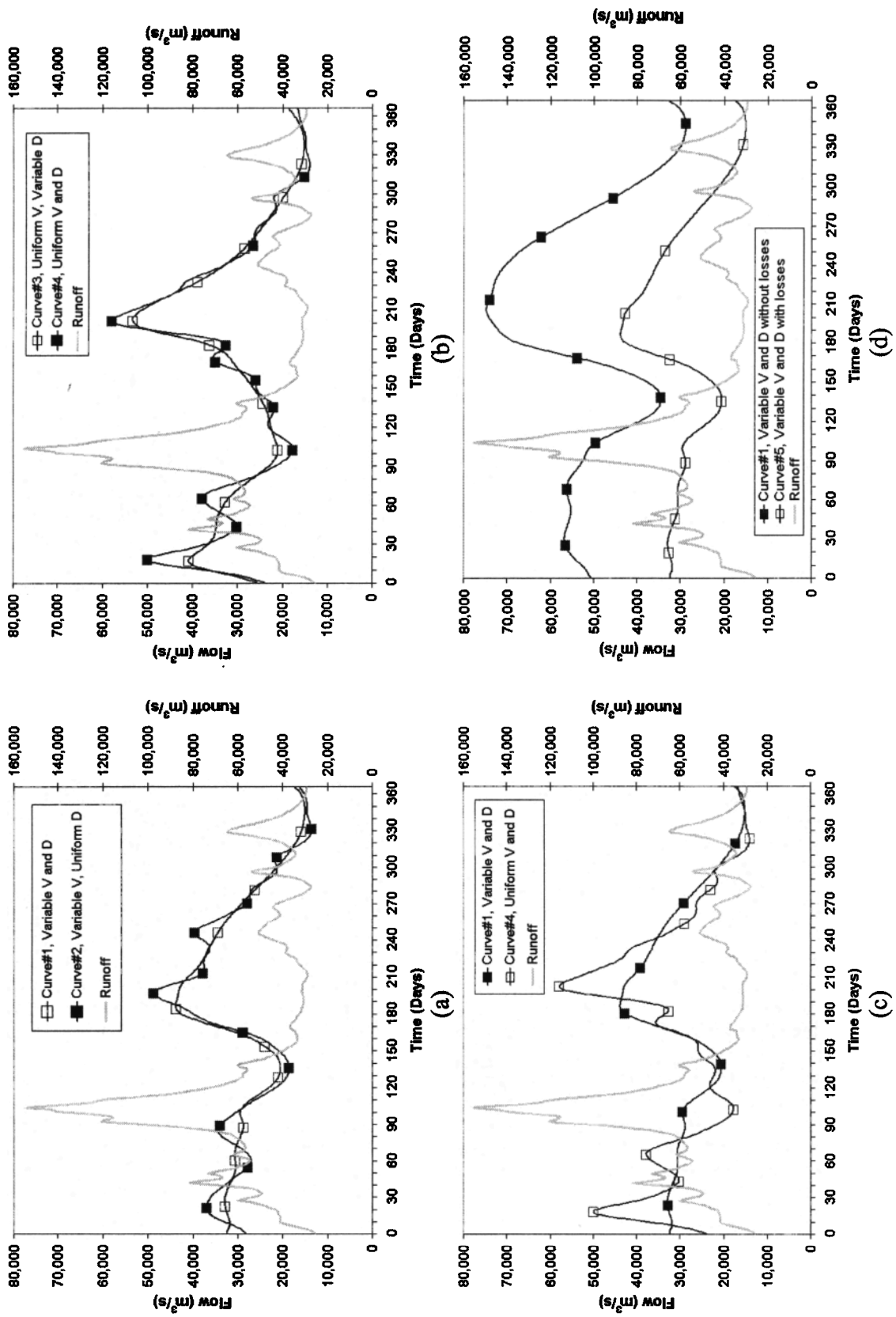

Figure 9. Simulated 1-year hydrographs for the Nile River basin under different assumptions of flow velocity, attenuation coefficient, and loss parameters.

cies are retained solely for the purpose of preventing discontinuities in (18). Moreover, when an insignificant kinetic species is retained, the concentration of that species is small, due to the cutoff criteria. Thus the contribution of the retained kinetic species to changes in chemical speciation is small, and the rate of reaction at this point is quite slow because of (15).

There are two precipitated kinetic species ($Fe(OH)_3(s)$ and $MnO_2(s)$) associated with the reaction network used in this effort (see Table 2). Since the precipitated species are immobile, they do not need a transport equation. However, the precipitated species may be composed of components that are not present in all compartments (see Table 3). In this paper the component Mn is only present in compartments 2 and 3 (for $MnO_2(s)$ and associated aqueous complexes), and the component Fe is only present in compartment 3 (for $Fe(OH)_3(s)$ and associated aqueous complexes). Again, there is the potential for discontinuities in transport equations that could be handled with moving boundaries. This time, however, it is (16) that could encounter a discontinuity at compartment boundaries, because the transported entities (i.e., dissolved Mn and Fe) are components, not kinetic species. A strategy similar to that used for aqueous kinetic species is employed. Since the incoming water is pristine (i.e., in compartment 1), Mn and Fe are defined as having a dissolved concentration of zero at the upstream boundary but an initial condition throughout the spatial domain that consists solely of precipitated concentration. This allows T_{Mn} and T_{Fe} to be continuous across the spatial domain because of (17).

2.2.3. Linkage. Inspection of (2) and (3) reveals that there is yet another potential for discontinuities in T_j during the course of redox zone development. This type of discontinuity cannot be handled in a manner similar to the kinetic species because it occurs with components that are present in all compartments. The cause of this discontinuity is that some components may experience a large change in value at compartmental boundaries. Clearly, such discontinuities would wreak havoc on most numerical methods for solute transport. An alternative formulation for the compartmentalized approach that circumvents this problem is

$$T_j^n = T_j^1 + \sum_{i=1}^{R_n} a_{ij} y_i^n \big|_{y_i^n \neq y_i^1} - \sum_{i=1}^{n-1} s_{(n-1)j}^h x_{n-1}^h \qquad (19)$$

$$n = 1,\ k;\ j = 1,\ N_c.$$

When simulating perturbed redox systems, it can usually be assumed that the dissolved redox species are either initially zero or initially the maximum value for that particular setting. For these conditions, it can be shown that (19) is equivalent to (2) through (4). As an example, consider the reaction network outlined in Table 2. Expanding (2) and (3) for the total analytical concentration of H^+ in compartment 2 yields

$$T_{H^+}^2 = -\mathrm{ALK} + 2[CO_2]_T - [MnO_2(s)]_T + 2[O_2(aq)]^\circ - 2[O_2(aq)]. \qquad (20)$$

Expanding (19) for the total analytical concentration for H^+ in compartment 2 yields

$$T_{H^+}^2 = -\mathrm{ALK} + 2[CO_2]_T + 2[O_2]_T - [MnO_2(s)]_T - 2[O_2(aq)]. \qquad (21)$$

Since $[O_2(aq)]^\circ = [O_2]_T$, (20) and (21) are equivalent.

When (19) is used to account for compartmental switching, one simply transports only T_j^1 for components subject to large changes between compartments (in this paper H^+ and CO_3^{2-}). This alternative formulation for the compartmentalized approach eliminates the discontinuities associated with (2)–(4); T_j^n is calculated from (19) and then passed to the chemical module.

2.2.4. Flowchart of COMPTRAN. COMPTRAN was constructed with extensively modified versions of the geochemical code KEMOD [*Yeh et al.*, 1993, 1998] and the coupled solute transport/geochemical code HYDROGEOCHEM 2.1 [*Yeh and Salvage*, 1995]. HYDRAQL [*Papelis et al.*, 1988] was incorporated within COMPTRAN to perform the equilibrium calculations.

All of the solute transport simulations performed in this effort were conducted with COMPTRAN. The flowchart in Figure 2 illustrates how COMPTRAN operates. Only the major subroutines are shown in Figure 2. It should be pointed out that each one of the subroutines shown in Figure 2 (except for truth.f) contains calls to other subroutines to perform various tasks related to the primary purpose of the calling routine. The new routines that were developed and the HYDROGEOCHEM 2.1 routines that were modified for this study are represented, respectively, by the dark gray and light gray rectangles in Figure 2.

In addition to performing geochemical and solute transport calculations, COMPTRAN essentially works by making two key decisions. The first decision to be made is to assign each node to the correct compartment. This decision is made by the subroutine switch.f (Figure 2a). The sequence of operations that is followed each time ocspit.f is called by gm2d.f is illustrated in the flowchart in Figure 2b. The subroutine ocspit.f loops over the entire set of nodes in the boundary value problem and calculates a "batch" geochemical solution at each node. The second major decision is made within the geochemical sequence of operations. A decision is made within the subroutine truth.f as to whether the lower-energy redox reaction within a given compartment is behaving in a kinetically limited or thermodynamically limited manner. This decision is made by determining whether the concentration of the lower-energy redox product is lower in the kinetic step or in the thermodynamic step (see Figure 1): (1) If the concentration of the lower-energy redox product is lower in the kinetic step, then the reaction is kinetically limited. (2) If the concentration of the lower-energy redox product is lower in the thermodynamic step, then the reaction is being limited by free energy constraints.

2.3. Elimination of Transport Equations

Depending on how the geochemical problem is formulated, it may not be necessary to write a transport equation (i.e., equation (16)) for each component. Recall that the global mass of a component is reaction-invariant and is also independent of other components. The compartmentalized approach allows the definition of at least one reaction network in which the total analytical concentration (i.e., T_j) of some components does not change. If a particular T_j does not change in time and space, the transport equation for that T_j can be dropped from the system of equations under consideration.

Consider a pristine aquifer governed by oxic compartment conditions, in which the components are H^+, CO_3^{2-}, NO_3^-, and "CH_2O" and oxygen reduction and denitrification are the only redox reactions. By definition, these reactions cannot change